catalysts

MDPI

Article

Scalability of U-Shape Magnetic Nanoparticles-Based Microreactor–Lipase-Catalyzed Preparative Scale Kinetic Resolutions of Drug-like Fragments

Fausto M. W. G. Silva [1], Ali O. Imarah [1,2], Orsolya Takács [1], László Tuba [1] and László Poppe [1,3,4,*]

[1] Department of Organic Chemistry and Technology, Budapest University of Technology and Economics, Műegyetem rkp. 3, H-1111 Budapest, Hungary
[2] Chemical Engineering Department, College of Engineering, University of Babylon, Hilla Babylon 5100, Iraq
[3] Biocatalysis and Biotransformation Research Center, Faculty of Chemistry and Chemical Engineering, Babeş-Bolyai University of Cluj-Napoca, Arany János Str. 11, RO-400028 Cluj-Napoca, Romania
[4] SynBiocat Ltd., Szilasliget u 3, H-1172 Budapest, Hungary
* Correspondence: poppe.laszlo@vbk.bme.hu; Tel.: +36-(1)-463-3299

Abstract: The production of active pharmaceutical ingredients (APIs) and fine chemicals is accelerating due to the advent of novel microreactors and new materials for immobilizing customized biocatalysts that permit long-term use in continuous-flow reactors. This work studied the scalability of a tunable U-shape magnetic nanoparticles (MNPs)-based microreactor. The reactor consisted of a polytetrafluoroethylene tube (PTFE) of various inner diameters (ID = 0.75 mm, 1.50 mm, or 2.15 mm) and six movable permanent magnets positioned under the tube to create reaction chambers allowing the fluid reaction mixture to flow through and above the enzyme-loaded MNPs anchored by permanent magnets. The microreactors with various tube sizes and MNP capacities were tested with the preparative scale kinetic resolution of the drug-like alcohols 4-(3,4-dihydroisoquinolin-2(1*H*)-yl)butan-2-ol (±)-**1a** and 4-(3,4-dihydroquinolin-1(2*H*)-yl)butan-2-ol (±)-**1b,** utilizing Lipase B from *Candida antarctica* immobilized covalently onto MNPs, leading to highly enantioenriched products [(*R*)-**2a,b** and (*S*)-**1a,b**]. The results in the U-shape MNP flow reactor were compared with reactions in the batch mode with CaLB-MNPs using similar conditions. Of the three different systems, the one with ID = 1.50 mm showed the best balance between the maximum loading capacity of biocatalysts in the reactor and the most effective cross-section area. The results showed that this U-shaped tubular microreactor might be a simple and flexible instrument for many processes in biocatalysis, providing an easy-to-set-up alternative to existing techniques.

Keywords: magnetic nanoparticles; flow biocatalysis; lipase; kinetic resolution; microreactor; chiral 3D *N*-heterocycle

Citation: Silva, F.M.W.G.; Imarah, A.O.; Takács, O.; Tuba, L.; Poppe, L. Scalability of U-Shape Magnetic Nanoparticles-Based Microreactor–Lipase-Catalyzed Preparative Scale Kinetic Resolutions of Drug-like Fragments. *Catalysts* **2023**, *13*, 384. https://doi.org/10.3390/catal13020384

Academic Editors: Pawel Borowiecki, Dominik Koszelewski and Evangelos Topakas

Received: 27 November 2022
Revised: 30 January 2023
Accepted: 8 February 2023
Published: 10 February 2023

1. Introduction

Due to the extensive substrate specificity, good selectivity, mild reaction conditions, and environmentally friendly nature, biocatalysis is a field that has gained increased attention in recent years in the chemical, pharmaceutical, cosmetic, food industries, and medicinal areas [1,2].

Among these biocatalysts, lipases (EC 3.1.1.3) represent a class of enzymes—produced by various sources, including animal, vegetable, and microbiological ones—with the inherent ability to hydrolyze fats and lipids. In addition to hydrolysis, they can catalyze interesterification, transesterification, esterification, alcoholysis, acidolysis, and aminolysis processes [3]. The lipases generally have a very broad substrate range and recognize a variety of non-natural substrates, which makes them appealing for applications in different sectors. One of their most important applications is the synthesis of enantiopure active pharmaceutical ingredients (APIs) in the pharma industry, by exploiting the kinetic resolution approach, in which

one enantiomer is selectively converted over the other with high enantiomeric selectivity, producing highly enantiopure APIs [4,5].

One of the most often employed enzymes in biocatalytic applications is the lipase B from *Candida antarctica* (CaLB)—which exhibits strong catalytic activity towards a wide range of substrates with variable size and polarity with remarkable activity, selectivity, and stability in various processes such as hydrolysis, transesterifications, Michael addition, and so on—to prepare compounds that are particularly valuable for drug development [6–8].

Immobilization may improve the enzyme's stability and ability to manufacture pure products [9–11]. It may also improve storage stability and reduce the environmental burden by making the biocatalyst separation and recovery easier, thereby significantly lowering operational expenses. Immobilization techniques utilized for CaLB include adsorption, the covalent approach, entrapment [12,13], and cross-linked enzyme aggregates [14]. These processes are performed using several different matrices and supports, such as silica and derivates [15–17], carbon nanotubes [18,19], and magnetic nanoparticles (MNPs) [20,21].

The MNP-based methods can benefit from the magnetic separability of the particles from various chemical and biological materials at the micro- and nanoscale [22–24]. They bring many advantages, which may be useful in biomedical applications and the pharmacological field, including small size, large surface-to-volume ratio enabling improved adsorption, and potential for manipulating them magnetically [25]. MNPs can undergo easy surface modification through functionalization with different materials providing further benefits such as strong enzyme affinity and binding [23,24,26]. Understandably, MNPs and their derivatives are beneficial supports for enzyme immobilization.

Various forms of CaLB immobilized by the aid of MNPs (CaLB-MNPs) were utilized as biocatalysts in a variety of applications such as the deacidification of rice bran oil [27], biodiesel production from waste oil [28–30], the production of flavor esters [31], and diverse hydrolysis and esterification reactions [32–34], including the kinetic resolution and dynamic kinetic resolution of racemic compounds [20,35–37].

Even today, batch reactors are used most frequently in the pharmaceutical sector to produce APIs [38–40]. However, upscaling batch processes from the laboratory scale to larger scale requires substantial redesign. Microreactor technology using flow chemistry—applying a system continuously injecting a fluid containing the starting material through the reactor, resulting in a product stream—contributes to the simplification of the main challenges of scaling up [38–41]. Flow chemistry has several benefits including the ease of control and automation, the capacity to execute reactions that are challenging or very difficult to make in batch mode in a safer way, and the enhanced selectivity, eco-friendliness, and sustainability [40]. The flow systems, based mostly on microreactor technology, can potentially improve about 50% of all chemical processes [42].

Microreactor technology is developing more and more in enzyme biotechnology and biocatalysis for biocatalyst screening, evolution, and other high-throughput biocatalytic processes. The manufacturing of pharmaceuticals and fine chemicals beneficially utilizes immobilized and tailored biocatalysts, enabling long-term use in reactors operating under a continuous flow regime [43]. Enzymatic microreactors—such as microfluidics chips, capillary microreactors, and microtube reactors—become valuable instruments for analytical processes [44], for kinetic studies of immobilized enzymes [45] and for parameter optimization in biocatalysis and biotransformations [46], for example for the kinetic resolution (KR) of secondary alcohols [47]. In the microreactor area, aiming tunable, scalable, and versatile reactors, 3D printing proved to be a useful tool [48].

Several studies combined the benefits of microreactor technology and the immobilization of biocatalysts on magnetic nanoparticles for various diagnostic applications [49,50] or for multipurpose applications, such as the microfluidic multiple-cell chip reactor filled with enzyme-coated MNPs [51,52]. Microreactors applying MNP biocatalysts enabled compartmentalization during small-scale biotransformation assays [53]. A magnetic oscillation microfluidic chip optimization of operating conditions for His-tagged enzymes immobilized on affinity MNPs was utilized for the stereoselective synthesis of chiral com-

pounds [54]. Recently, an easy-to-create MNP-based PTFE tube microreactor with six adjustable permanent magnets under the tube was applied for the CaLB-MNP-catalyzed enantiomer selective acylation of racemic alcohol, 4-(morpholin-4-yl)butan-2-ol in continuous flow mode [55].

Inspired by the work on the use of the simple U-shape flow reactor [55], the main goal of this study was to test the scalability of this simple MNP flow microreactor by applying reactor body tubes of different inner diameters filled with different amounts of MNP biocatalyst. Since CaLB-MNP-catalysis in the simple U-shape MNP reactor was efficiently applicable for the small-scale KR of a drug-like secondary alcohol comprising a nonplanar *N*-heterocyclic part [55], in this work, the scalability of the U-shape MNP-based microreactor was tested with the CaLB-MNP-catalyzed preparative scale kinetic resolution of further secondary alcohols as drug-like fragments.

2. Results and Discussion

The assessment of the structural features of active pharmaceutical ingredients (APIs) of commercialized drugs showed that the most abundant ring fragment within APIs was the phenyl ring. The aromatic phenyl ring is the most typical 2D fragment, since it contains only sp^2-hybridized heavy atoms resulting in the planarity of the ring. The further ring fragments in the following three positions are saturated heterocycles such as morpholine, piperidine, and piperazine [56]. These rings can be termed as 3D fragments because they all contain at least one sp^3-hybridized heavy atom, rendering them nonplanar. An analysis of the drug-likeness of various molecules revealed that the presence of such nonplanar fragments—resulting in less rigid and sterically more complex molecular skeletons—enhanced the drug-likeness of the API candidates without significantly increasing the molecular weight [57]. The easiness of the preparation of racemic 4-(morpholyn-4-yl)butan-2-ol through the aza-Michael reaction of the *N*-heterocycle and methyl vinyl ketone followed by a simple sodium borohydride reduction of the formed ketone [55] inspired us to extend this methodology to synthesize further 3D-fragment-containing 4-(*N*-heterocycle-substituted)butan-2-ols analogously. Thus, the racemic secondary alcohol substrates for this study were prepared with the straightforward two-step aza-Michael addition of the 3D *N*-heterocycles isoquinoline or quinoline (HcNH, in Scheme 1) to methyl vinyl ketone/sodium borohydride reduction synthesis sequence leading via the corresponding ketones **3a,b** to the desired racemic 4-(3,4-dihydroisoquinolin-2-(1*H*)-yl)butan-2-ol (±)-**1a** and 4-(3,4-dihydroquinolin-1-(2*H*)-yl)butan-2-ol (±)-**1b** (Scheme 1).

*2.1. Kinetic Resolution of Racemic 4-(3,4-Dihydroisoquinolin-2-(1H)-yl)butan-2-ol (±)-***1a** *and 4-(3,4-Dihydroquinolin-1-(2H)-yl)butan-2-ol (±)-***1b** *with CaLB-MNP Biocatalyst in Batch Mode*

The biocatalyst chosen for this scalability study was the robust lipase B from *Candida antarctica* immobilized by covalent binding onto magnetic nanoparticles (CaLB-MNPs), because this form proved to be efficient and stable in various reaction modes including the convenient U-shape MNP microreactor [55]. Thus, the applicability and scalability of the U-shape MNP reactor were studied using the kinetic resolution of synthesized secondary alcohols (±)-**1a** and (±)-**1b** with vinyl acetate and CaLB-MNPs in batch and continuous flow modes (Scheme 1).

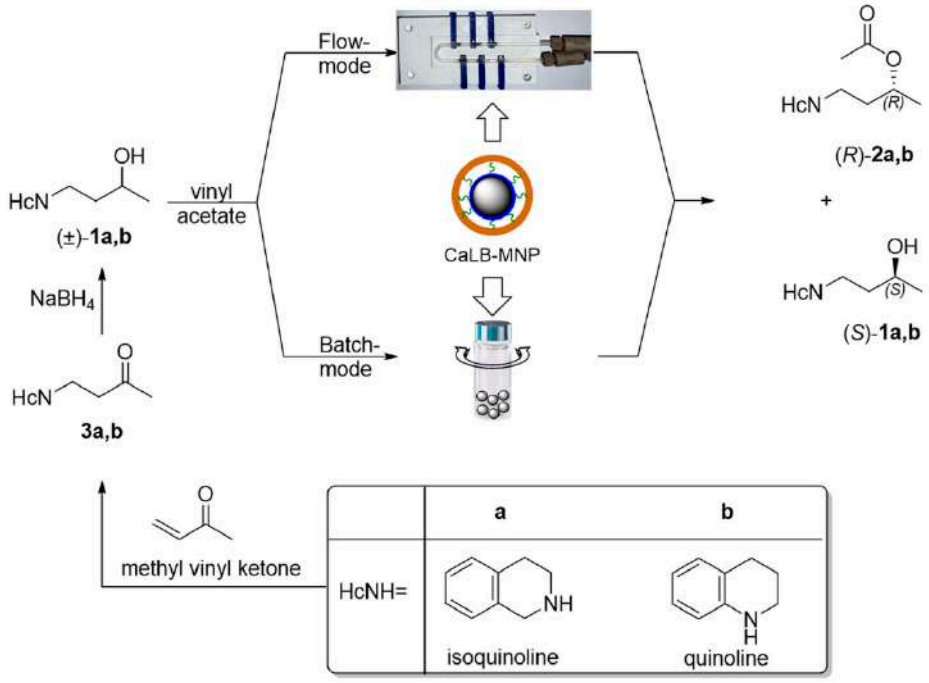

Scheme 1. Synthesis and kinetic resolution of racemic 4-(3,4-dihydroisoquinolin-2-(1*H*)-yl)butan-2-ol (±)-**1a** or 4-(3,4-dihydroquinolin-1-(2*H*)-yl)butan-2-ol (±)-**1b** catalyzed by lipase B from *Candida antarctica* (CaLB) immobilized on magnetic nanoparticles (MNPs) in batch and continuous flow mode.

Our efforts to analyze the enantiomeric composition of the products by GC were successful only partially since we could separate the enantiomers of the acetates (±)-**2a** and (±)-**2b**) only but not of the alcohols (±)-**1a** and (±)-**1b**) (see Sections S1.2. and S4. of Supplementary Materials). Nevertheless, the calculation of the enantiomeric ratio (*E*) characterizing the degree of enantiomer selectivity in the irreversible KR processes (Ref. [58]: $E = k_{(R)}/k_{(S)}$) was feasible by using the conversion (*c*) and enantiomeric composition of the product fractions (ee_P).

First, the time course of the KRs in batch mode was analyzed at four different substrate concentrations (12.5 mM, 25 mM, 50 mM, and 100 mM for both (±)-**1a** and (±)-**1b**)) for 24 h (Figure 1).

Apparently, the kinetic resolution of the isoquinoline-containing alcohol (±)-**1a** (Figure 1a) was slower than that of the quinoline-derived substrate (±)-**1b** (Figure 1b). The KR process from (±)-**1a** achieved 50% conversion after 24 h only at the lower substrate concentrations (12.5 mM and 25 mM) but not at the higher concentrations (50 mM or 100 mM) (Figure 1a). The observation of conversion higher than 50% of the racemate indicated that the enantiomer selectivity of the process favoring the (*R*)-enantiomer [(*R*)-**1a**] was not exclusive. This was confirmed by the enantiomeric ratio (*E*) [58] calculated for the process indicating a high but not outstanding value (*E* ~125 ± 28 within all the four series of experiments from (±)-**1a**). Accordingly, the enantiopurity of the forming enantiomer remained in the 96–98%ee range even at small degrees of conversion. The absolute configuration of the product (*R*)-**2b** was assigned by analogy with the (*R*)-configuration of the faster-reacting enantiomer of the isosteric 4-phenybutan-2-ol [59] or 4-(morpholyn-4-yl)butan-2-ol [55] and was confirmed using our established calculation method [60].

On the other hand, the kinetic resolution of the quinoline derivative (±)-**1b** (Figure 1b) was faster, achieving 50% conversion after 6 h at the lowest substrate concentration (12.5 mM) and after 24 h at the highest substrate concentration (100 mM). Like the KR of isoquinoline-containing alcohol (±)-**1a,** the enantiomer selectivity of the CaLB-MNP-catalyzed acylation of the quinoline-containing alcohol (±)-**1b** was high but not exclusive (*E* ~104 ± 32 within all the four series of experiments from (±)-**1b**), indicated

also by the conversions from racemates exceeding 50% at substrate concentrations below 50 mM.

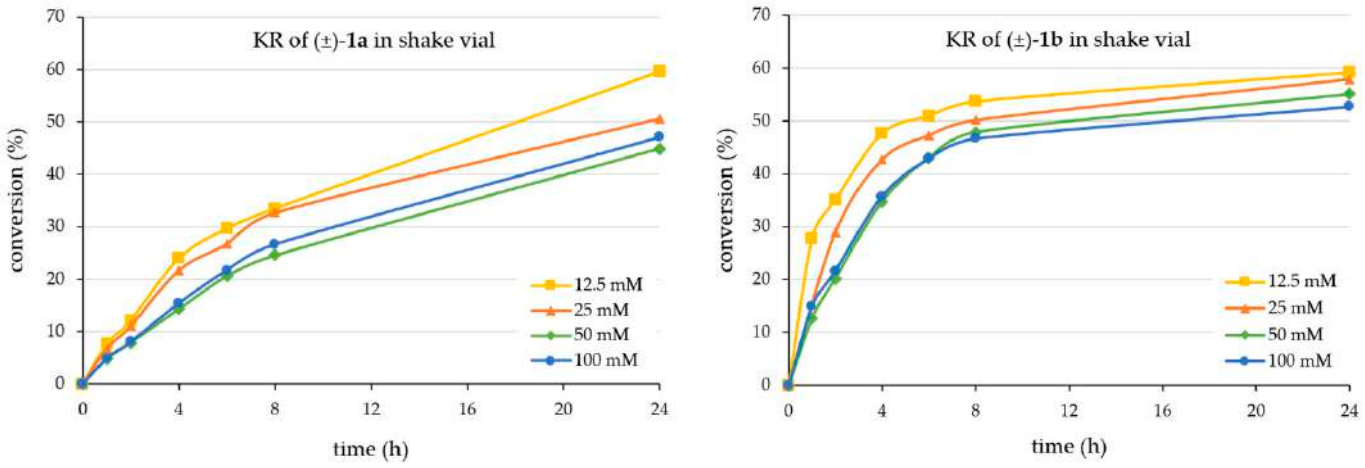

(**a**) (**b**)

Figure 1. Time course of the CaLB-catalyzed kinetic resolution with vinyl acetate in batch mode using as substrate (**a**) the racemic 4-(3,4-dihydroisoquinolin-2(1*H*)-yl)butan-2-ol (±)-**1a** or (**b**) the racemic 4-(3,4-dihydroquinolin-1(2*H*)-yl)butan-2-ol (±)-**1b** (for details, see Section 3.3).

Based on these results, preparative scale KRs of racemic (±)-**1a** and (±)-**1b** were performed at 25 mM substrate concentration (Table 1). First, the CaLB-MNP-catalyzed KR of the isoquinoline-containing alcohol (±)-**1a** was performed at 25 °C utilizing a 1:20 mass ratio of substrate to CaLB-MNP, resulting in the (*R*)-acetate [(*R*)-**2a**] with high enantiopurity (96.7%ee) and the less reactive alcohol enantiomer [(*S*)-**1a**] in moderate enantiomeric excess (76%ee; using the $ee_{(S)\text{-}\mathbf{1a}} = c \times ee_{(R)\text{-}\mathbf{2a}}/(1 - c)$ equation and the experimental c and $ee_{(R)\text{-}\mathbf{2a}}$ values) after 90 h from a reaction achieving 44% of conversion. The isolation involving preparative TLC allowed the excellent (~94%) recovery of the ester fraction (*R*)-**2a** and less efficient (~31%) recovery of the alcohol fraction (*S*)-**1a**. Interestingly, the sign of optical rotation for the alcohol (*S*)-**1a** switched from negative at 356 nm to positive at 578 nm. The wavelength dependence of the optical rotation for the ester (*R*)-**2a** was much less pronounced (the negative value at 365 nm decreased to 68% at 578 nm but without changing the sign).

Table 1. Kinetic resolution of racemic 4-(3,4-dihydroisoquinolin-2(1H)-yl)butan-2-ol (±)-**1a** and racemic 4-(3,4-dihydroquinolin-1(2*H*)-yl)butan-2-ol (±)-**1b** catalyzed by CaLB-MNP in batch mode.

Subst.	Time (h)	Temp. (°C)	Conv. (%)	Product	Yield [1] (%)	*ee* [2] (%)	*E* [3]	$[\alpha]_{365}$ [4]	$[\alpha]_{578}$ [4]
(±)-**1a**	90	25	44	(*R*)-**2a**	41.3	96.7	137	+9.1	+6.2
		25	44	(*S*)-**1a**	17.5	76.0 [5]	137	−6.4	+1.8
(±)-**1b**	30	25	41	(*R*)-**2b**	29.2	96.8	126	−29.8	−0.3
		25	41	(*S*)-**1b**	13.1	67.3 [5]	126	+3.6	+12.2
(±)-**1b**	36	20	38	(*R*)-**2b**	24.6	97.9	180	−27.3	−0.3
(±)-**1b**	75	20	49	(*R*)-**2b**	41.2	95.4	136	−26.8	−0.4
(*S*)-**1b**	[6]	[6]	[6]	(*S*)-**2b** [6]	60.2	87.2		+24.3	+0.3

[1] From kinetic resolution of the corresponding substrate in batch mode after reaching the conversion as indicated ((±)-**1a** or (±)-**1b** (410 mg), CaLB-MNP (20 mg) and vinyl acetate (500 µL) in MTBE-hexane mixture (1:2 ratio, 10 mL) in a vial at 20 °C shaken in orbital shaker at 600 rpm). [2] Determined by chiral GC (see Supplementary Materials) [3] Calculated from the conversion (c) and enantiomeric excess of the product fraction ($ee_{(R)\text{-}\mathbf{2}}$) according to Chen et al. [58]. [4] Determined at 20 °C (c = 3, in ethanol). Acetate **2a,b** samples were measured immediately after dissolving. [5] Calculated from the conversion (c) and enantiomeric ratio by the $ee_{(S)\text{-}\mathbf{1}} = c \times ee_{(R)\text{-}\mathbf{2}}/(1 - c)$ equation. [6] Prepared by acetylation of (*S*)-**1b** (obtained after 49% conversion, using AcCl/5M NaOH in ethyl acetate: see Sections S3.6 and S3.7 of Supplementary Materials).

Next, the CaLB-MNP-catalyzed KR of the faster-reacting quinoline-containing alcohol (±)-**1b** was performed at 25 °C utilizing a 1:20 mass ratio of substrate to CaLB-MNP as well. This KR achieved reasonable conversion (41%) in a much shorter reaction time (30 h) as was required for the isoquinoline-containing alcohol. The degree of enantiomer selectivity was similar for the KRs from the two alcohols (E = 137 from (±)-**1a**; E = 126 from (±)-**1b**)), allowing isolation of the (*R*)-acetate [(*R*)-**2b**] also in high enantiopurity (96.8%ee) with good recovery (71%) and the less reactive (*S*)-alcohol [(*S*)-**1b**] in moderate enantiomeric excess (67.3%ee; calculated from experimental c and $ee_{(R)\text{-}\mathbf{2a}}$ values) with lower recovery (22%). To enhance enantiopurity, the temperature was lowered to 20 °C using lower conversion for the ester (*R*)-**2b** with improved *ee*, and higher conversion for the residual alcohol (*S*)-**1b** in higher *ee*. As expected, higher enantiomer selectivity was found (E = 180 and 136, for the reactions conducted for 38% and 49% conversions, respectively) and at lower conversion (38%), it was possible to enhance the enantiomeric excess of (*R*)-**2b** to 97.9%ee (from 96.8%ee at c = 41%), while at higher conversion (49%), the enantiopurity of (*S*)-**1b** improved to 87.2%ee (from 67.3%ee at c = 41%). The significant wavelength dependence of the optical rotation could be observed in this case as well. The optical rotations for both the ester (*R*)-**2b** and the alcohol (*S*)-**1b** were significantly higher at 365 nm than at 578 nm but without changing the sign.

*2.2. Kinetic Resolution Experiments with Racemic 4-(3,4-Dihydroisoquinolin-2(1H)-yl)butan-2-ol (±)-***1a** *and 4-(3,4-Dihydroquinolin-1(2H)-yl)butan-2-ol (±)-***1b** *in Continuous Flow Mode U-Shape Reactor Utilizing CaLB-MNPs*

Since CaLB-MNP-catalysis in the simple U-shape MNP reactor was efficiently applicable for the small-scale KR of the drug-like racemic 4-(morpholyn-4-yl)butan-2-ol comprising a nonplanar *N*-heterocyclic part [55], in this work, the scalability of the U-shape MNP-based microreactor was tested further with the CaLB-MNP-catalyzed KRs of the drug-like 3D *N*-heterocycle-containing 4-(3,4-dihydroisoquinolin-2(1*H*)-yl)butan-2-ol (±)-**1a** and 4-(3,4-dihydroquinolin-1(2*H*)-yl)butan-2-ol (±)-**1b**. The previously designed convenient U-shape reactor made of a PTFE tube and six adjustable permanent magnets [55] was modified, enabling variation in the inner diameter (ID) of the tube (Figure 2).

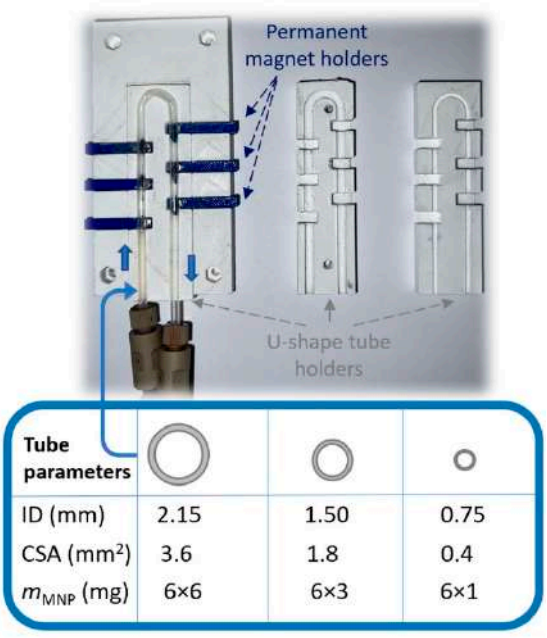

Figure 2. A close-up of the variable MNP-based flow reactor comprising exchangeable U-shape tube holders capable of keeping reaction tubes of three different inner diameters (IDs = 2.15 mm, 1.50 mm, and 0.75 mm) and six removable permanent magnets within the tubes to create reaction cells of different size and MNP biocatalyst-anchoring capacity.

The goal of these investigations was to vary the capacity of the maximum MNP biocatalyst's loading in one reactor cell and determine and compare the operation parameters without significant leaching—essentially, the process where a catalyst is lost in the fluid reaction—of the biocatalyst (Figure 3). For the PTFE tube of 0.75 mm ID (cross-sectional area (CSA) ~0.44 mm^2), 6 mg of CaLB-MNPs was distributed in six reaction chambers. To preserve the loading ratio, 18 mg (6 × 3 mg) and 36 mg (6 × 6 mg) CaLB-MNPs were applied in the 1.50 mm ID (CSA ~1.8 mm^2) and 2.15 mm ID (CSA ~3.6 mm^2) reactors, respectively. With the variable U-shape reactor in our hand, the continuous flow KR of the drug-like *N*-heterocyclic alcohols (±)-**1a** and (±)-**1b** was performed at 25 °C using various flow rates between 1 and 3 µL min^{-1} (Figure 3a,b).

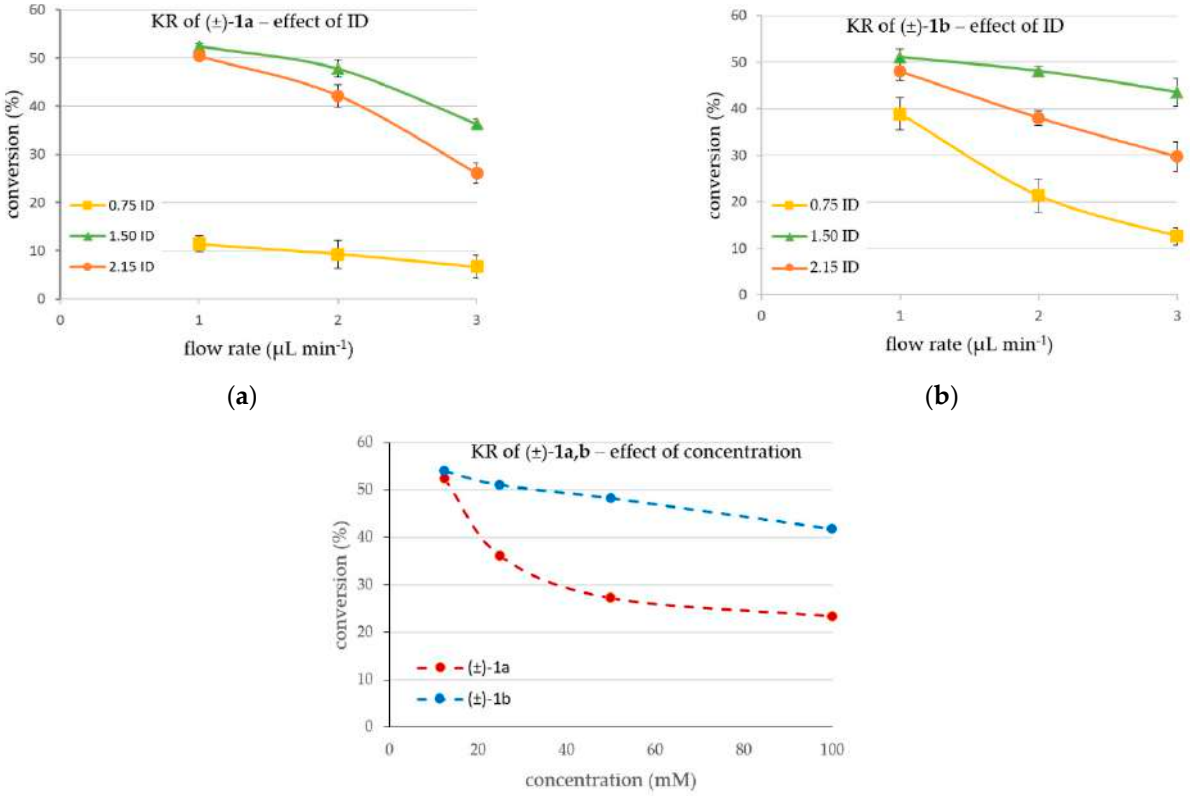

Figure 3. CaLB-MNP-catalyzed kinetic resolution in continuous flow mode within U-shape MNP tube reactors of three different inner diameters at various flow rates using vinyl acetate as acylating agent and (**a**) the racemic 4-(3,4-dihydroisoquinolin-2(1H)-yl)butan-2-ol (±)−**1a** (12.5 mM) or (**b**) the racemic 4-(3,4-dihydroquinolin-1(2*H*)-yl)butan-2-ol (±)−**1b** (25 mM) (in MTBE-hexane 1:2, vinyl acetate (31.25 mM for (±)−**1a**, 62.5 mM for (±)−**1b**), 25 °C) as substrate. Effect of (**c**) concentration of (±)−**1a**,**b** on the conversion of the KR processes in the flow reactor with optimal diameter (ID = 1.5 mm, at flow rate of 1 µL min^{-1}).

It is considered that after finding the optimal tube diameter, numbering up the cells seems easily implementable. A logical setup is to use the wave shape (consisting more of U turns) reactor setup. For example, 9 turns with 10 cells after each turn would represent a 100-cell reactor holding up to 3.6 g of the MNP biocatalyst within a less than 2 m long tube fitting onto a less than 20 cm × 20 cm plate. Such a plate would represent a multigram-scale reactor, and such gram scale reactors are easily parallelizable with standard joining elements. The U-shape reactor in this study approaches the first part of this geometry.

Due to the different activity of the CaLB-MNP biocatalyst towards the two investigated racemic alcohols (±)-**1a** and (±)-**1b** observed in the batch mode (Figure 2 and Table 1), the influence of the three different reactor sizes on the KRs was tested at different substrate con-

centrations. Since the batch mode experiments revealed the KR of 4-(3,4-dihydroisoquinolin-2(1H)-yl)butan-2-ol (±)-**1a** as slower than of the 4-(3,4-dihydroquinolin-1(2*H*)-yl)butan-2-ol (±)-**1b**, a lower concentration (12.5 mM) was applied for (±)-**1a** (12.5 mM, Figure 3a) than for (±)-**1b** (25 mM, Figure 3b) enabling it to reach 50% conversion from the corresponding racemates quite conveniently within a short time.

The results indicated that highest conversions could be obtained in the 1.50 mm tube setup with both substrates (Figure 3a,b). This can be explained by the insufficient amount of biocatalyst per cell in the 0.75 mm tube reactor—although the flow could provide full contact with the MNP-CaLBs, as shown in Figure 4a—meaning that this amount of biocatalyst gets saturated with the substrate, resulting in low conversion values. In the narrow 0.75 mm tube reactor, leaching also happened at the highest flow rate due to the too-tight packing of MNPs and the highest linear velocity of the flow. Additionally, in the case of too-tight packing, there is an increased possibility of microchannel formation among the MNP particles, negatively influencing the efficiency. In the 2.15 mm tube system, the tube is too wide, and the permanent magnet's field is not strong enough to keep the MNPs well distributed along the full cross-section area (Figure 4c). Consequently, the possibility of leaching could be increased, and a significant portion of the flow could pass through the reaction chamber without direct contact with the CaLB-MNP-filled space. This effect decreased the rate of reaction considerably because from the fraction of fluid flowing without directly contacting the MNP biocatalyst, just the diffusion allows the substrate to reach the biocatalyst.

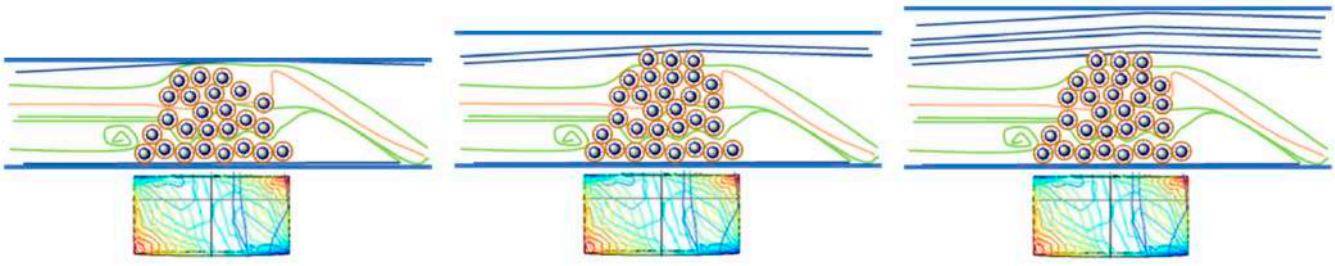

(**a**) (**b**) (**c**)

Figure 4. Schematic behavior of a CaLB-MNP-containing reaction cell in a tubular MNP flow reactor with tubes of different inner diameter (the rectangles below the tubes of various diameters show the polarity and magnetic field withing the same permanent magnet). Panel (**a**) depicts the case when the tube is too narrow, panel (**b**) shows an ideal case where the quantity of biocatalysts fits the tube size, while panel (**c**) illustrates a case where the tube is too wide.

Presumably, the 1.50 mm tube system approaches the best ideal case (Figure 4b) where the quantity of the MNP biocatalysts is sufficient for being not fully saturated, and the tube size allows almost full contact with the MNP-filled area, but the linear velocity of the liquid remains below the limit which causes leaching problems.

Leaching, essentially the process where a catalyst is lost in the fluid reaction, is a major problem in flow chemistry processes [61]. The loading of biocatalyst particles influences the flow because with the dispersion of MNPs provoked by the magnetic field, a certain area of the biocatalyst is in contact with the through-flowing reaction medium. In small diameters, leaching can happen due to the tight MNP biocatalyst loading and high linear velocity of the liquid. When the diameter of the tube increases, the distance between the magnetic nanoparticles and the permanent magnet also increases, weakening the anchoring forces keeping the MNPs in the reaction chamber. Leaching of the particles being distant from the permanent magnet can happen even at quite low linear velocities, which can result in a loss of the biocatalysts (Figure 4c).

Data in Figure 3 clearly show that the specific activity of the CaLB-MNPs is the best in the 1.50 mm tube system under each condition. For example, in the KRs of (±)-**1a** at the flow rate of 1 μL min^{-1} (Figure 3a), the 3-fold higher amount of CaLB-MNP in the 1.50 mm

reactor as compared to the 0.75 mm reactor (18 mg vs. 6 mg) led to 52.4% conversion, which was 4.6-fold higher than was observed in the 0.75 mm system (11.4%), meaning 1.5-fold higher specific activity. On the other hand, the specific activity of CaLB-MNP in the 1.50 mm reactor allowing 52.4% conversion with 18 mg of the biocatalyst was more than twofold higher than in the 2.15 mm system since the somewhat lower 50.3% conversion in the 2.15 mm reactor was reached with double the amount of biocatalyst (36 mg). Worth noting is that, in all cases, the 1.50 mm system provided the highest conversion.

After finding the optimal setup for the inner diameter (1.50 mm) and flow rate (1 μL min^{-1}), the effect of the concentration of the substrates (±)-**1a** and (±)-**1b** on the KR in the continuous flow setup was investigated (Figure 3c). The results were in line with the observed differences between the KR processes with (±)-**1a** and (±)-**1b** in batch mode (Figure 1a,b, respectively). It was apparent that at a low (12.5 mM) substrate concentration, the specific activity of CaLB-MNP was high enough to achieve ≥50% conversion. The more significant drop in conversion with increasing concentration of (±)-**1a** as compared to (±)-**1b** can be rationalized by assuming that the Michaelis constant of (±)-**1b** may be lower (K_M < 50 mM) than that of (±)-**1a** (K_M > 50 mM).

Next, the operational stability of the system under the optimal conditions (ID = 1.50 mm, flow rate = 1 μL min^{-1}) was studied with the 100 mM concentration of the substrates (±)-**1a**,**b** at 20 °C for 48 h (Figure 5a,b).

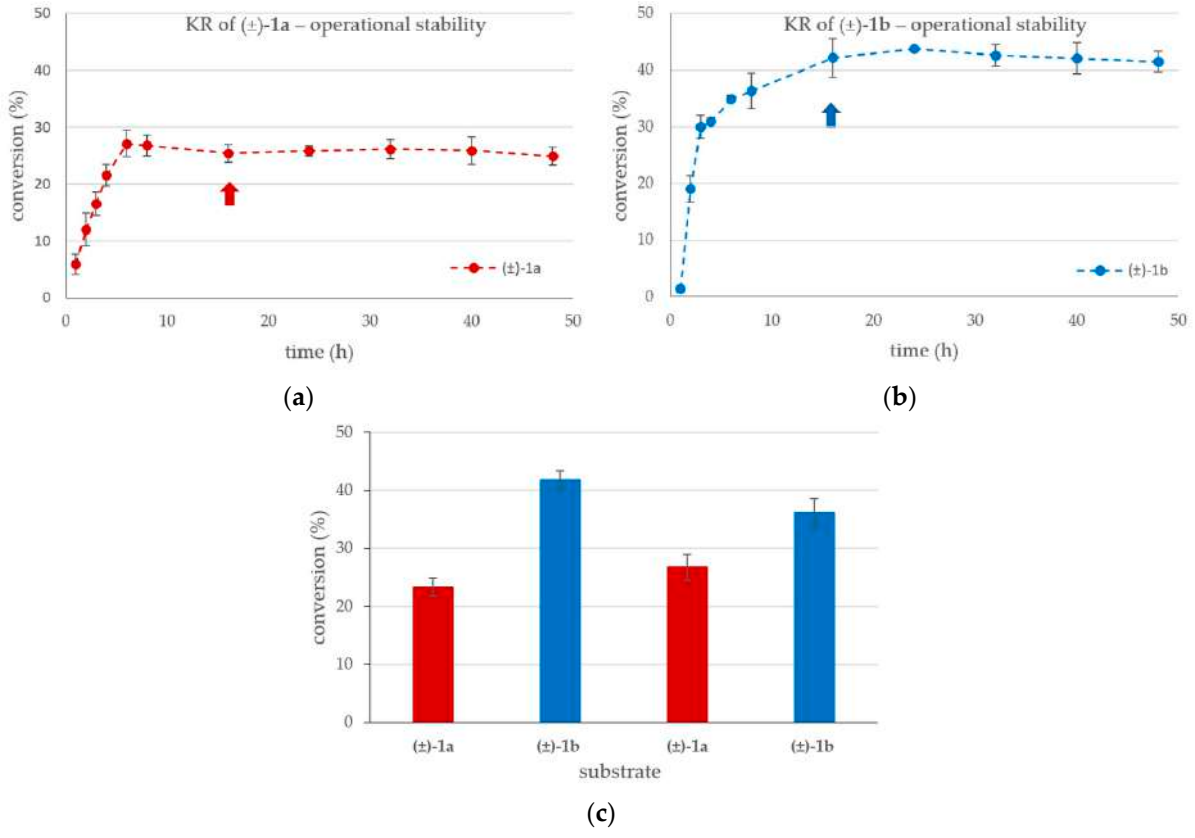

Figure 5. Time course of the KRs at 100 mM substrate concentration in the U-shape reactor (ID = 1.5 mm) with (**a**) the racemic 4-(3,4-dihydroisoquinolin-2(1H)-yl)butan-2-ol (±)-**1a**, or with (**b**) the racemic 4-(3,4-dihydroquinolin-1(2*H*)-yl)butan-2-ol (±)-**1b** (in MTBE-hexane 1:2, vinyl acetate (250 mM), 20 °C, 1 μL min^{-1}). Interchange (**c**) of the KRs of racemic (±)-**1a** and (±)-**1b** in four alternating cycles (the arrows in Panels a and b correspond the reaction times of the cycles in Panel c). The bars represent the conversion for (±)-**1a** (red) and for (±)-**1b** (blue) in the reaction mixture after 16 h long run at 20 °C (washing with solvent for 1 h at 5 μL min^{-1} was applied between cycles).

The high substrate concentration was selected for these series of investigations because, at lower conversions (~25–28% for (±)-**1a**; and ~41–44% for (±)-**1b**), the operational stability study is more visible if the conversion remains far below the theoretical limit of a fully selective KR (50%). It is notable that the KR of (±)-**1a** stabilized after 6 h, while for (±)-**1b,** more than 12 h was required to reach the stationary state. After stabilization, the KR process remained stable with both substrates for at least 24 h, up to the 48-h length of time of this study. During the long-term runs of the U-shape reactor used to investigate the steady-state stabilization (Figure 5a,b), the outflowing reaction mixture was collected between the 16th-40th h (~1.5 mL). The products isolated from this mixture (Table 2) were indistinguishable from those isolated from the KR of (±)-**1** in batch mode.

Table 2. Continuous flow kinetic resolution of racemic 4-(3,4-dihydroisoquinolin-2(1*H*)-yl)butan-2-ol (±)-**1a** and racemic 4-(3,4-dihydroquinolin-1(2*H*)-yl)butan-2-ol (±)-**1b** catalyzed by CaLB-MNPs.

Subst.	Conv. [1] (%)	Product	Yield (%)	*ee* [2] (%)
(±)-**1a**	25.4	(*R*)-**2a**	21	93.1
	25.4	(*S*)-**1a**	36 [3]	[4]
(±)-**1b**	43.7	(*R*)-**2b**	39	91.8
	43.7	(*S*)-**1b**	34 [3]	[4]

[1] From kinetic resolution of the corresponding substrate in U-shape reactor (ID = 1.5 mm, 18 mg of CaLB-MNPs) after reaching stationary state ((±)-**1a** or (±)-**1b** (100 mM), vinyl acetate (250 mM) in MTBE-hexane mixture (1:2 ratio) at 20 °C and at flow rate of 1 μL min^{-1}) collected for 24 h. [2] Determined by chiral GC (see Supplementary Materials) [3] The high polarity of the alcohol enabled only noncomplete recovery of (*S*)-**1a** from the silica gel during preparative TLC. [4] The *ee* of (*S*)-**1a** and (*S*)-**1b** could not be detected directly using GC.

To investigate the reusability of the CaLB-MNP preparation in the U-shape reactor system (ID = 1.50 mm), four cycles of 17 h long experiments—reaction runs with 100 mM (±)-**1a** or (±)-**1b** at 1 μL min^{-1} for 16 h, exceeding the time required reaching the stationary state, followed by washing with substrate-free solvent with 5 μL min^{-1} flow rate for 1 h—were performed (Figure 5c). The results of KRs with alternating substrates demonstrated the recyclability of the CaLB-MNP biocatalyst from one reaction to another one.

Finally, the space time yields (STY) in the KR processes starting from 100 mM (±)-**1a**,**b** could be compared [55]. The KR process in batch mode revealed STY_B = 0.9 mmol L^{-1} h^{-1} and 1.9 mmol L^{-1} h^{-1} for the acetate formation ((*R*)-**2a** and (*R*)-**2b**, respectively). When the KR process was performed in continuous flow mode in the U-shape reactor (ID = 1.5 mm) and considering the total U-shape volume ($V_{U\text{-}shape}$ = 236 μL), an $STY_{U\text{-}shape}$ = 1.6 mmol L^{-1} h^{-1} and 2.8 mmol L^{-1} h^{-1} could be determined for (*R*)-**2a** and (*R*)-**2b**, respectively. However, considering only the volume of the MNP-filled reaction chambers ($V_{U\text{-}shape}$ = 56 μL) of the U-shape MNP reactor, an STY_{filled} = 6.7 mmol L^{-1} h^{-1} and 11.6 mmol L^{-1} h^{-1} for (*R*)-**2a** and *R*)-**2b**, respectively, could be calculated.

3. Materials and Methods

3.1. Materials

The details regarding materials and solvents, the origin of recombinant lipase B from *Candida antactica* (CaLB), and the synthesis of 4-(3,4-dihydroisoquinolin-2(1*H*)-yl)butan-2-ol (±)-**1a**, 4-(3,4-dihydroquinolin-1(2*H*)-yl)butan-2-ol (±)-**1b**, 4-(3,4-dihydroisoquinolin-2(1*H*)-yl)butan-2-yl acetate (±)-**2a**, 4-(3,4-dihydroquinolin-1(2H)-yl)butan-2-yl acetate (±)-**2b**, 4-(3,4-dihydroisoquinolin-2(1*H*)-yl)butan-2-one **3a**, and 4-(3,4-dihydroquinolin-1(2H)-yl)butan-2-one **3b** are given as supplementary information.

The following sections were analogous to previously published methods [55] with minor modifications, as detailed below.

3.2. Analytical and Separation Methods

The optical rotations were measured on a Perkin-Elmer 241 polarimeter at two different lines of mercury (at 365 nm and 578 nm) in ethanol (the acetates **2a,b** were measured

immediately after dissolving). The polarimeter was calibrated with measurements of both enantiomers of menthol.

NMR spectra were recorded in the indicated deuterated solvents on Bruker DRX-500 or DRX-300 spectrometers operating at 500 MHz or 300 MHz for ^{1}H, and 126 or 75 MHz for ^{13}C. NMR signals are given in ppm on the δ scale.

Infrared (IR) spectra were recorded on a Bruker ALPHA FT-IR spectrometer (in ATR mode), and wavenumbers (ν) of bands are listed in cm^{-1}.

The gas chromatographic (GC) analyses were performed with an Agilent 4890 gas chromatograph equipped with FID detector using H_2 carrier gas (injector: 250 °C, detector: 250 °C, head pressure: 12 psi, and split ratio: 50:1) using a Hydrodex β-6TBDM column (25 m × 0.25 mm × 0.25 μm film of heptakis-(2,3-di-*O*-methyl-6-*O*-*t*-butyldimethylsilyl)- β-cyclodextrin; Macherey & Nagel). The details on the method used and the retention times of components in the kinetic resolution reactions are given in Table S1 in the Supplementary Materials.

*3.3. Assaying the Kinetic Resolution of 4-(3,4-Dihydroisoquinolin-2(1H)-yl)butan-2-ol (±)-***1a** *and 4-(3,4-Dihydroquinolin-1(2H)-yl)butan-2-ol (±)-***1b** *by CaLB-MNP Biocatalyst in Batch Mode*

The activity assays were performed in clean screw-capped vials (4 mL) using CaLB-MNPs (5 mg) as a biocatalyst in the reaction mixture containing various concentrations (12.5 mM, 25 mM, 50 mM, or 100 mM) of racemic 4-(3,4-dihydroisoquinolin-2(1*H*)-yl)butan-2-ol (±)-**1a** or 4-(3,4-dihydroquinolin-1(2*H*)-yl)butan-2-ol (±)-**1b** and vinyl acetate (31.5 mM, 62.5 mM, 125 mM, or 250 mM, respectively) in a mixture of methyl *t*-butyl ether (MTBE)-hexane (1:2 ratio, 1 mL).

For sampling, aliquots (20 μL) taken from the reaction mixtures were diluted with ethanol (480 μL) and analyzed using GC as described in Section 3.2.

*3.4. Kinetic Resolution of 4-(3,4-Dihydroisoquinolin-2(1H)-yl)butan-2-ol (±)-***1a** *and 4-(3,4-Dihydroquinolin-1(2H)-yl)butan-2-ol (±)-***1b** *by CaLB-MNPs Biocatalyst at Preparative Scale in Batch Mode*

Into a 20 mL screw-cap vial, the racemic substrate 4-(3,4-dihydroisoquinolin-2(1*H*)-yl)butan-2-ol (±)-**1a** or 4-(3,4-dihydroquinolin-1(2*H*)-yl)butan-2-ol (±)-**1b** (410 mg, 2 mmol; in all cases), CaLB-MNPs (20 mg), and vinyl acetate (500 μL) were added to a mixture of methyl t-butyl ether (MTBE)-hexane (1:2 ratio, 10 mL), and the resulting suspension was shaken at room temperature (as detailed in Table 1) in a Vibramax 100 shaker (Heidolph, Schwabach, Germany) for the reaction time indicated in Table 1. The CaLB-MNPs were removed by anchoring with a neodymium magnet and decanting the supernatant. The resuspended CaLB-MNPs were washed with a mixture of methyl *t*-butyl ether (MTBE)-hexane (1:2 ratio, 2 × 2.5 mL), dried in a fume hood overnight at room temperature, and stored in a refrigerator until further use. After removing the volatiles from the combined solutions via vacuum rotary evaporation, the resulting products were separated with preparative thin-layer chromatography (silica gel, eluted with CH_2Cl_2:MeOH 20:1) to give the formed (*R*)-acetate (*R*)-**2a** or (*R*)-**2b** and the residual (*S*)-alcohol (*S*)-**1a** or (*S*)-**1b**, respectively.

3.4.1. 4-(3,4-Dihydroisoquinolin-2(1*H*)-yl)butan-2-yl Acetate (*R*)-**2a**

Yield: 200.9 mg, 41.3%. Amber oil.

$[\alpha]_{365}^{20}$ = +9.1 and $[\alpha]_{578}^{20}$ = +6.2 (*c* 3, EtOH) for the sample with an *ee* = 96.7% from GC. IR (ATR, film, cm^{-1}): 3023, 2923, 1734, 1496, 1455, 1371, 1239, 1131, 1097, 1017, 740 cm^{-1}. ^{1}H NMR (500 MHz, $CDCl_3$) δ 7.14 (qd, *J* = 6.3, 3.1 Hz, 3H), 7.07–7.02 (m, 1H), 5.02 (ddd, *J* = 7.6, 6.3, 5.2 Hz, 1H), 2.96 (t, *J* = 6.0 Hz, 2H), 2.82 (t, *J* = 6.0 Hz, 2H), 2.67–2.60 (m, 1H), 1.98 (dddd, *J* = 13.6, 9.5, 7.6, 6.1 Hz, 1H), 1.87 (ddd, *J* = 13.7, 9.5, 4.7 Hz, 1H), 1.32–1.26 (m, 7H). ^{13}C NMR (126 MHz, $CDCl_3$) δ 170.7, 133.9, 128.7, 126.6, 126.4, 125.8, 69.6, 55.8, 54.3, 50.8, 33.3, 29.7, 28.6, 21.4, 20.2.

3.4.2. 4-(3,4-Dihydroisoquinolin-2(1*H*)-yl)butan-2-ol (*S*)-**1a**

Yield: 71.6 mg, 17.5%. Amber oil.

$[\alpha]_{365}^{20} = -6.4$ and $[\alpha]_{578}^{20} = +1.8$ (*c* 3, EtOH) for the sample with an *ee* = 76.0% (via calculation from *c* and $ee_{(R)\text{-}\mathbf{2a}}$). IR (ATR, film, cm^{-1}): 3354, 3065, 3023, 2965, 2965, 2809, 1599, 149, 1455, 1372, 1342, 1134, 1092, 935, 740 cm^{-1}. ^{1}H NMR (500 MHz, $CDCl_3$) δ 7.20–7.14 (m, 2H), 7.13 (dt, *J* = 6.3, 3.7 Hz, 1H), 7.05 (dd, *J* = 7.1, 1.9 Hz, 1H), 4.51 (s, 1H), 4.03 (ddd, *J* = 9.0, 6.1, 2.6 Hz, 1H), 3.88 (d, *J* = 14.9 Hz, 1H), 3.78 (d, *J* = 15.0 Hz, 1H), 3.11–3.04 (m, 1H), 2.98 (d, *J* = 6.1 Hz, 2H), 2.97–2.89 (m, 1H), 2.89–2.76 (m, 2H), 1.79 (tt, *J* = 9.7, 4.6 Hz, 1H), 1.68 (dtd, *J* = 14.6, 4.6, 2.5 Hz, 1H), 1.24–1.19 (m, 3H). ^{13}C NMR (126 MHz, $CDCl_3$) δ 133.9, 133.4, 132.8, 128.7, 126.7, 126.6, 126.1, 68.8, 56.5, 55.6, 50.2, 33.5, 31.2, 28.0, 27.0, 23.5.

3.4.3. 4-(3,4-Dihydroquinolin-1(2*H*)-yl)butan-2-yl Acetate (*R*)-**2b**

Yield: 142 mg, 29.2%

$[\alpha]_{365}^{20} = -29.8$ and $[\alpha]_{578}^{20} = -0.3$ (*c* 3, EtOH) for the sample with an *ee* = 96.8% from GC. IR (ATR, film, cm^{-1}): 3065, 3017, 2929, 2843, 1733, 1601, 1504, 1457, 1370, 1237, 1121, 1019, 741 cm^{-1}. ^{1}H NMR (500 MHz, $CDCl_3$) δ 7.08 (td, *J* = 7.8, 1.8 Hz, 1H), 7.00–6.95 (m, 1H), 6.61 (t, *J* = 7.7 Hz, 2H), 4.99 (tdd, *J* = 7.6, 5.6, 1.5 Hz, 1H), 3.42–3.24 (m, 4H), 2.78 (t, *J* = 6.4 Hz, 2H), 2.09 (s, 3H), 1.98 (dq, *J* = 6.8, 2.3 Hz, 2H), 1.88 (dt, *J* = 8.3, 4.3 Hz, 2H), 1.29 (d, *J* = 6.3 Hz, 3H. ^{13}C NMR (126 MHz, $CDCl_3$) δ 170.7, 129.3, 127.1, 116.6, 69.4, 49.5, 47.8, 32.3, 29.7, 28.0, 21.4, 20.3.

3.4.4. 4-(3,4-Dihydroquinolin-1(2*H*)-yl)butan-2-ol (*S*)-**1b**

Yield: 53.8, mg, 13.1%

$[\alpha]_{365}^{20} = +3.6$ and $[\alpha]_{578}^{20} = +12.2$ (*c* 3, EtOH) for the sample with an *ee* = 67.3% (via calculation from *c* and $ee_{(R)\text{-}\mathbf{2a}}$). IR (ATR, film, cm^{-1}): 3372, 3063, 3020, 2925, 2864, 1601, 1504, 1456, 1345, 1302, 1208, 1129, 1061, 740 cm^{-1}. ^{1}H NMR (500 MHz, $CDCl_3$) δ 7.13–7.06 (m, 1H), 6.98 (dd, *J* = 7.3, 1.6 Hz, 1H), 6.77–6.71 (m, 1H), 6.64 (t, *J* = 7.3 Hz, 1H), 3.97 (dtd, *J* = 10.9, 6.3, 5.1, 2.5 Hz, 1H), 3.43 (ddt, *J* = 16.0, 14.6, 8.2 Hz, 2H), 3.31 (dq, *J* = 15.5, 5.8 Hz, 2H), 2.79 (t, *J* = 6.4 Hz, 2H), 2.01–1.95 (m, 2H), 1.82–1.71 (m, 2H), 1.27 (d, *J* = 6.2 Hz, 4H). ^{13}C NMR (126 MHz, $CDCl_3$) δ 145.5, 129.3, 127.1, 123.2, 117.1, 112.5, 66.9, 49.5, 49.2, 35.4, 28.0, 24.1, 22.7.

3.5. Design and Assembly of the U-Shape MNP Reactor

The U-shape MNP reactor system (Figure 2) was designed by the AutoCAD (2020 student version) program and printed with a Rankfor100 3D printer (CEI Conrad Electronic International, Ltd., New Territories, Hong Kong). This study used neodymium disc magnets, 4 mm × 2 mm, N35 (Euromagnet Ltd., Budapest, Hungary) as permanent magnets, and polytetrafluoroethylene (PTFE) tubes with ID 0.75 mm, 1.50 mm, and 2.15 mm as the reactor body and connection parts. The inner part of the U-shape reactor was a proper exchangeable holder allowing the adjustable positioning of six permanent magnets in the closest possible vicinity to the PTFE tube reactor, thereby creating six sites where the magnets could anchor the CaLB-MNPs biocatalysts inside the tube (Figure 2). A SpinSplit continuous flow syringe pump (SpinSplit Technical Research and Development LLC, Budapest, Hungary) equipped with two glass syringes of 0–5 mL volume was coupled to the tubular reactor part of the reactor module.

*3.6. Kinetic Resolution of 4-(3,4-Dihydroisoquinolin-2(1H)-yl)butan-2-ol (±)-***1a** *and 4-(3,4-Dihydroquinolin-1(2H)-yl)butan-2-ol (±)-***1b** *by CaLB-MNPs Biocatalysts in the Continuous Flow U-Shape Reactor*

The variable U-shape reactor was used for the continuous flow kinetic resolution of the designed substrate alcohols (±)-**1a** and (±)-**1b** with PTFE reactor tubes of different IDs (0.75 mm, 1.50 mm, and 2.15 mm). Different quantities of CaLB-MNPs (6 × 1 mg, 6 × 3 mg, and 6 × 6 mg for IDs of 0.75 mm, 1.50 mm, and 2.15 mm, respectively) were suspended in 1 mL of a mixture of methyl *t*-butyl ether (MTBE)-hexane (1:2 ratio) for the different reactor

tubes, and the suspended CaLB-MNPs were supplied at a 50 μL min^{-1} flow rate into the reactor's six chambers in the counter-current direction of the later fluid flow, filling the last chamber first and the first chamber last.

Experiments were performed by pumping solutions of the substrate 4-(3,4-dihydroisoquinolin-2(1*H*)-yl)butan-2-ol (±)-**1a** (12.5 mM) and 4-(3,4-dihydroquinolin-1(2*H*)-yl)butan-2-ol (±)-**1b** (25 mM), and vinyl acetate (31.5 or 62.5 mM, respectively) in a mixture of methyl t-butyl ether (MTBE)-hexane (1:2 ratio) through the U-shape reactor filled with CaLB-MNPs at various flow rates (1, 2, 3 μL min^{-1}) at 25 °C.

For the series of experiments of reusability of the CaLB-MNP preparation in the U-shape reactor system (ID = 1.50 mm), four alternating cycles of 17 h long experiments composed of reaction runs with 100 mM (±)-**1a** or (±)-**1b**, and vinyl acetate (250 mM) in a mixture of methyl *t*-butyl ether (MTBE)–hexane (1:2 ratio) at 1 μL min^{-1} for 16 h were conducted, followed by washing with a substrate-free solvent with 5 μL min^{-1} flow rate for 1 h at 20 °C.

For the preparative scale experiment, the U-shape MNP tube reactor was fed with racemic 4-(3,4-dihydroisoquinolin-2(1*H*)-yl)butan-2-ol (±)-**1a** or 4-(3,4-dihydroquinolin-1(2*H*)-yl)butan-2-ol (±)-**1b** (205 mg, 1 mmol, each) and vinyl acetate (924 μL, 2.5 equiv.) in 10 mL of solution with MTBE–hexane 1:2 as the solvent at a flow rate of 1 μL min^{-1}. After collecting the outflowing solutions during a 24 h period, the volatiles were removed using vacuum rotary evaporation and the resulting products were separated with preparative thin-layer chromatography (silica gel, eluted with CH_2Cl_2:MeOH 20:1) to give the formed (*R*)-acetate (*R*)-**2a** or (*R*)-**2b** and the residual (*S*)-alcohol (*S*)-**1a** or (*S*)-**1b**, respectively.

The analysis of the collected samples was carried out similarly as described for the KRs in batch mode (see Section 3.3).

3.6.1. 4-(3,4-Dihydroisoquinolin-2(1*H*)-yl)butan-2-yl Acetate (*R*)-**2a**

Yield: 9 mg, 21% for the sample with an *ee* = 93.1% from GC.

3.6.2. 4-(3,4-Dihydroisoquinolin-2(1*H*)-yl)butan-2-ol (*S*)-**1a**

Yield: 22 mg, 36%.

3.6.3. 4-(3,4-Dihydroquinolin-1(2*H*)-yl)butan-2-yl Acetate (*R*)-**2b**

Yield: 15.5 mg, 39% for the sample with an *ee* = 91.8% by GC.

3.6.4. 4-(3,4-Dihydroquinolin-1(2*H*)-yl)butan-2-ol (*S*)-**1a**

Yield: 16.6 mg, 34%.

4. Conclusions

This study performed kinetic resolutions of the drug-like fragments 4-(3,4-dihydroisoquinolin-2(1*H*)-yl)butan-2-ol (±)-**1a** and 4-(3,4-dihydroquinolin-1(2*H*)-yl)butan-2-ol (±)-**1b** with Lipase B from *Candida antarctica* immobilized on MNPs in batch and in continuous flow modes. The batch mode KRs showed the usefulness of these substrates for the preparation of the enantiomeric forms (the acetates (*R*)-**2a,b** and the alcohols (S)-**1a,b**) in moderate-to-high enantiomeric excess and allowed the thorough characterization of the novel compounds including their absolute configuration and optical rotation.

The kinetic resolutions of the compounds (±)-**1a** and (±)-**1b** in an enhanced version of a U-shape MNP-based continuous flow microreactor with variable inner-diameter tubing proved that, in this type of reactor, the effectivity of the CaLB-MNP biocatalyst could be enhanced compared to the reaction made in the batch mode.

In the continuous flow mode, the most important consideration was to avoid the MNP biocatalyst leaching at relatively high loading within the reactor tubes of different inner diameters (0.75 mm, 1.50 mm, and 2.15 mm). The experiments at various flow rates (1–3 μL min^{-1}) with the alcohol solutions (12.5 mM of (±)-**1a** and 25 mM of (±)-**1b**) revealed that in the investigated flow rate regime, the tube with a 1.50 mm ID resulted in the highest

conversions and best specific biocatalyst activities, because this tube size allowed good filling capacity without leaching but with good MNP distribution, providing efficient contact between the reaction medium and the MNP particles. The possibility of being scalable enhanced the usefulness of this MNP-based U-shape tubular continuous flow microreactor as a handy and adaptable tool for further diverse biotechnological processes.

Supplementary Materials: The following supporting information can be downloaded at: https://www.mdpi.com/article/10.3390/catal13020384/s1: Materials and methods for the preparation of CaLB-MNP biocatalyst [55,62]; Synthesis of the racemic alcohols (±)-**1a**, (±)-**1b** and the racemic acetates (±)-**2a**, (±)-**2b** and (S)-acetate (*S*)-**2b** [63–66]; Table S1: GC method and retention times for analysis of the kinetic resolution reactions by chiral GC; Figures S1–S32: GC chromatograms, ^{1}H- and ^{13}C-NMR, and IR spectra of compounds (±)-**1a,b**, (±)-**2a,b**, (*R*)-**2a,b**, (*S*)-**1a,b** and (*S*)-**2b**; Figures S33–S36: typical GC chromatograms for the KRs of (±)-**1a,b** in batch mode and in the continuous flow U-shape reactor.

Author Contributions: Conceptualization, F.M.W.G.S., A.O.I. and L.P.; methodology, F.M.W.G.S. and A.O.I.; validation, L.P.; investigation, F.M.W.G.S., A.O.I., L.T. and O.T.; resources, L.P.; writing—original draft preparation, F.M.W.G.S.; writing—review and editing, F.M.W.G.S. and L.P.; visualization, F.M.W.G.S. and L.P.; supervision, L.P.; funding acquisition, L.P. All authors have read and agreed to the published version of the manuscript.

Funding: The research reported in this paper is part of project no. TKP2021-EGA-02, implemented with the support provided by the Ministry for Innovation and Technology of Hungary from the National Research, Development and Innovation Fund, financed under the TKP2021 funding scheme. This work was also supported by a grant from the Romanian Ministry of Education and Research, CCCDI-UEFISCDI, project number PN-III-P2-2.1-PED-2019-5031, within PNCDI III. The PhD scholarships of F.M.W.G.S and A.O.I. were financed by the Stipendium Hungaricum Scholarship Program.

Data Availability Statement: Not applicable.

Acknowledgments: The authors gratefully acknowledge the technical assistance of Edit Tóth-Németh and József Szemes.

Conflicts of Interest: The authors declare no conflict of interest.

References

1. Yi, D.; Bayer, T.; Badenhorst, C.P.S.; Wu, S.; Doerr, M.; Höhne, M.; Bornscheuer, U.T. Recent trends in biocatalysis. *Chem. Soc. Rev.* **2021**, *50*, 8003–8049. [CrossRef] [PubMed]
2. Bell, E.L.; Finnigan, W.; France, S.P.; Green, A.P.; Hayes, M.A.; Hepworth, L.J.; Lovelock, S.L.; Niikura, H.; Osuna, S.; Romero, E.; et al. Biocatalysis. *Nat. Rev. Methods Prim.* **2021**, *1*, 46. [CrossRef]
3. Chandra, P.; Enespa; Singh, R.; Arora, P.K. Microbial lipases and their industrial applications: A compreenhesive review. *Microb. Cell Fact.* **2020**, *19*, 169. [CrossRef] [PubMed]
4. Contesini, F.J.; Davanço, M.G.; Borin, G.P.; Vanegas, K.G.; Cirino, J.P.G.; de Melo, R.R.; Mortensen, U.H.; Hildén, K.; Campos, D.R.; Carvalho, P.d.O. Advances in Recombinant Lipases: Production, Engineering, Immobilization and Application in the Pharmaceutical Industry. *Catalysts* **2020**, *10*, 1032. [CrossRef]
5. Kamble, M.P.; Yadav, G.D. Kinetic Resolution of (*R*,*S*)-α-Tetralol by Immobilized *Candida antarctica* Lipase B: Comparison of Packed-Bed over Stirred-Tank Batch Bioreactor. *Ind. Eng. Chem. Res.* **2017**, *56*, 1750–1757. [CrossRef]
6. Zhong, L.; He, C.; Xiao, C.; Yao, C.; Pyatt, I.H.; Lu, Y. Covalent Immobilization of *Candida antarctica* Lipase B on Functionalized Hollow Mesoporous Silica Nanoparticles. *ChemistrySelect* **2021**, *6*, 3453–3460. [CrossRef]
7. Palomo, J. Synthetic complexity created by lipases. *Nat. Catal.* **2020**, *3*, 335–336. [CrossRef]
8. Pérez-Venegas, M.; Juaristi, E. Mechanoenzymology: State of the Art and Challenges towards Highly Sustainable Biocatalysis. *ChemSusChem* **2021**, *14*, 2682–2688. [CrossRef]
9. Sheldon, R.A.; van Pelt, S. Enzyme immobilization in biocatalysis: Why, what and how. *Chem. Soc. Rev.* **2013**, *42*, 6223–6235. [CrossRef]
10. Zaitsev, S.Y.; Savina, A.A.; Zaitsev, I.S. Biochemical aspects of lipase immobilization at polysaccharides for biotechnology. *Adv. Colloid Interface Sci.* **2019**, *272*, 102016. [CrossRef]
11. Coşkun, G.; Çıplak, Z.; Yıldız, N.; Mehmetoğlu, Ü. Immobilization of *Candida antarctica* Lipase on Nanomaterials and Investigation of the Enzyme Activity and Enantioselectivity. *Appl. Biochem. Biotechnol.* **2021**, *193*, 430–445. [CrossRef] [PubMed]

12. Nicoletti, G.; Cipolatti, E.P.; Valério, A.; Carbonera, N.G.; Soares, N.S.; Theilacker, E.; Ninow, J.L.; de Oliveira, D. Evaluation of different methods for immobilization of *Candida antarctica* lipase B (CalB lipase) in polyurethane foam and its application in the production of geranyl propionate. *Bioprocess Biosyst. Eng.* **2015**, *38*, 1739–1748. [CrossRef] [PubMed]
13. Sigurdardóttir, S.B.; Lehmann, J.; Ovtar, S.; Grivel, J.-C.; Della Negra, M.; Kaiser, A.; Pinelo, M. Enzyme Immobilization on Inorganic Surfaces for Membrane Reactor Applications: Mass Transfer Challenges, Enzyme Leakage and Reuse of Materials. *Adv. Synth. Catal.* **2018**, *360*, 2578–2607. [CrossRef]
14. Saikia, K.; Rathankumar, A.K.; Vaithyanathan, V.K.; Cabana, H.; Vaidyanathan, V.K. Preparation of Highly Diffusible Porous Cross-Linked Lipase B from *Candida antarctica* Conjugates: Advances in Mass Transfer and Application in Transesterification of 5-Hydroxymethylfurfural. *Int. J. Biol. Macromol.* **2021**, *170*, 583–592. [CrossRef]
15. Cipolatti, E.P.; Rios, N.S.; Sousa, J.S.; Robert, J.D.M.; da Silva, A.A.T.; Pinto, M.C.; Simas, A.B.C.; Vilarrasa-García, E.; Fernandez-Lafuente, R.; Gonçalves, L.R.B.; et al. Synthesis of lipase/silica biocatalysts through the immobilization of CALB on porous SBA-15 and their application on the resolution of pharmaceutical derivatives and on nutraceutical enrichment of natural oil. *Mol. Catal.* **2021**, *505*, 111529. [CrossRef]
16. Wang, H.; Yue, W.; Zhang, S.; Zhang, Y.; Li, C.; Su, W. Modification of Silica Xerogels with Polydopamine for Lipase B from *Candida antarctica* Immobilization. *Catalysts* **2021**, *11*, 1463. [CrossRef]
17. Ficanha, A.M.M.; Antunes, A.; Oro, C.E.D.; Dallago, R.M.; Mignoni, M.L. Immobilization of *Candida antarctica* B (CALB) in Silica Aerogel: Morphological Characteristics and Stability. *Biointerface Res. Appl. Chem.* **2010**, *10*, 6744–6756. [CrossRef]
18. Sulym, I.; Zdarta, J.; Ciesielczyk, F.; Sternik, D.; Derylo-Marczewska, A.; Jesionowski, T. Pristine and Poly(Dimethylsiloxane) Modified Multi-Walled Carbon Nanotubes as Supports for Lipase Immobilization. *Materials* **2021**, *14*, 2874. [CrossRef]
19. Szelwicka, A.; Siewniak, A.; Kolanowska, A.; Boncel, S.; Chrobok, A. PTFE-Carbon Nanotubes and Lipase B from *Candida antarctica*—Long-Lasting Marriage For Ultra-Fast And Fully Selective Synthesis Of Levulinate Esters. *Materials* **2021**, *14*, 1518. [CrossRef]
20. Xing, X.; Jia, J.; Zhang, J.; Zhou, Z.; Li, J.; Wang, N.; Yu, X. CALB Immobilized onto Magnetic Nanoparticles for Efficient Kinetic Resolution of Racemic Secondary Alcohols: Long-Term Stability and Reusability. *Molecules* **2019**, *24*, 490. [CrossRef]
21. Monteiro, R.R.C.; Neto, D.M.A.; Fechine, P.B.A.; Lopes, A.A.S.; Gonçalves, L.R.B.; Dos Santos, J.C.S.; de Souza, M.C.M.; Fernandez-Lafuente, R. Ethyl Butyrate Synthesis Catalyzed by Lipases A and B from *Candida antarctica* Immobilized onto Magnetic Nanoparticles. Improvement of Biocatalysts' Performance under Ultrasonic Irradiation. *Int. J. Mol. Sci.* **2019**, *20*, 5807. [CrossRef] [PubMed]
22. Sheldon, R.A. Enzyme immobilization: The quest for optimum performance. *Adv. Synth. Catal.* **2009**, *349*, 1289–1307. [CrossRef]
23. Bilal, M.; Zhao, Y.; Rasheed, T.; Iqbal, H.M.N. Magnetic nanoparticles as versatile carriers for enzymes immobilization: A review. *Int. J. Biol. Macromol.* **2018**, *120*, 2530–2544. [CrossRef]
24. Matveeva, V.G.; Bronstein, L.M. Magnetic Nanoparticle-Containing Supports as Carriers of Immobilized Enzymes: Key Factors Influencing the Biocatalyst Performance. *Nanomaterials* **2021**, *11*, 2257. [CrossRef]
25. Flores-Rojas, G.G.; López-Saucedo, F.; Vera-Graziano, R.; Mendizabal, E.; Bucio, E. Magnetic Nanoparticles for Medical Applications: Updated Review. *Macromol* **2022**, *2*, 374–390. [CrossRef]
26. Slabu, I.; Galman, J.L.; Lloyd, R.C.; Turner, N.J. Discovery, Engineering, and Synthetic Application of Transaminase Biocatalysts. *ACS Catal.* **2017**, *7*, 8263–8284. [CrossRef]
27. Dong, T.; Zhou, X.; Dai, Y.; Yang, X.; Zhang, W.; Yu, D.; Liu, T. Application of magnetic immobilized enzyme of nano dialdehyde starch in deacidification of rice bran oil. *Enzym. Microb. Technol.* **2022**, *161*, 110116. [CrossRef] [PubMed]
28. Amini, Y.; Shahedi, M.; Habibi, Z.; Yousefi, M.; Ashjari, M.; Mohammadi, M. A multi-component reaction for covalent immobilization of lipases on amine-functionalized magnetic nanoparticles: Production of biodiesel from waste cooking oil. *Bioresour. Bioprocess.* **2022**, *9*, 60. [CrossRef]
29. Parandi, E.; Safaripour, M.; Abdellatiff, M.H.; Saidi, M.; Bozorgian, A.; Nodeh, H.R.; Rezania, S. Biodiesel production from waste cooking oil using a novel biocatalyst of lipase enzyme immobilized magnetic nanocomposite. *Fuel* **2022**, *313*, 123057. [CrossRef]
30. Mehrasbi, M.R.; Mohammadi, J.; Peyda, M.; Mohammadi, M. Covalent immobilization of *Candida antarctica* lipase on core-shell magnetic nanoparticles for production of biodiesel from waste cooking oil. *Renew. Energy* **2017**, *101*, 593–602. [CrossRef]
31. de Souza, M.C.M.; Dos Santos, K.P.; Freire, R.M.; Barreto, A.C.H.; Fechine, P.B.A.; Gonçalves, L.R.B. Production of flavor esters catalyzed by Lipase B from *Candida antarctica* immobilized on magnetic nanoparticles. *Braz. J. Chem. Eng.* **2017**, *34*, 681–690. [CrossRef]
32. Lee, H.Y.; Jang, W.Y.; Chang, J.H. Reusable and rapid esterolysis of nitrophenyl alkanoates with CalB enzyme-immobilized magnetic nanoparticles. *J. Korean Ceram. Soc.* **2022**, *59*, 527–535. [CrossRef]
33. Song, M.; Chang, J.-H. Thermally Stable and Reusable Ceramic Encapsulated and Cross-Linked CalB Enzyme Particles for Rapid Hydrolysis and Esterification. *Int. J. Mol. Sci.* **2022**, *23*, 2459. [CrossRef] [PubMed]
34. de Barros, H.R.; Tanaka, L.Y.; da Silva, R.T.P.; Santiago-Arcos, J.; Torresi, S.I.C.; López-Gallego, F. Assembly of Nano-Biocatalyst for the Tandem Hydrolysis and Reduction of *p*-Nitrophenol Esters. *Part. Part. Syst. Charact.* **2021**, *38*, 2100136. [CrossRef]
35. Netto, C.G.C.M.; Andrade, L.H.; Toma, H.E. Enantioselective transesterification catalysis by *Candida antarctica* lipase immobilized on superparamagnetic nanoparticles. *Tetrahedron Asymmetry* **2009**, *20*, 2299–2304. [CrossRef]

36. Spelmezan, C.G.; Bencze, L.C.; Katona, G.; Irimie, F.D.; Paizs, C.; Tosa, M.I. Efficient and Stable Magnetic Chitosan-Lipase B from *Candida antarctica* Bioconjugates in the Enzymatic Kinetic Resolution of Racemic Heteroarylethanols. *Molecules* **2020**, *25*, 350. [CrossRef]
37. Seddigi, Z.S.; Malik, M.S.; Ahmed, S.A.; Babalghith, A.O.; Kamal, A. Lipases in asymmetric transformations: Recent advances in classical kinetic resolution and lipase-metal combinations for dynamic processes. *Coord. Chem. Rev.* **2017**, *348*, 54–70. [CrossRef]
38. Hamidović, M.; Ender, F.; Springer, A.A. A Novel Enzymatic Microreactor: Towards Transforming the Pharmaceutical Industry. In *CMBEBIH 2019, IFMBE Proceedings*; Badnjevic, A., Škrbić, R., Gurbeta Pokvić, L., Eds.; Springer: Cham, Switzerland, 2020; Volume 73, pp. 303–308. [CrossRef]
39. Basso, A.; Serban, S. Industrial applications of immobilized enzymes—A review. *Mol. Catal.* **2019**, *479*, 110607. [CrossRef]
40. Baumann, M.; Moody, T.S.; Smyth, M.; Wharry, S. A Perspective on Continuous Flow Chemistry in the Pharmaceutical Industry. *Org. Process Res. Dev.* **2020**, *24*, 1802–1813. [CrossRef]
41. Britton, J.; Majumdar, S.; Weiss, G.A. Continuous flow biocatalysis. *Chem. Soc. Rev.* **2018**, *47*, 5891–5918. [CrossRef]
42. de Santis, P.; Meyer, L.-E.; Kara, S. The Rise of Continuous Flow Biocatalysis—Fundamentals, Very Recent Developments and Future Perspectives. *React. Chem. Eng.* **2020**, *5*, 2155–2184. [CrossRef]
43. Žnidaršič-Plazl, P. Biotransformations in microflow systems: Bridging the gap between academia and industry. *J. Flow Chem.* **2017**, *7*, 111–117. [CrossRef]
44. Nagy, C.; Szabo, R.; Gaspar, A. Microfluidic Immobilized Enzymatic Reactors for Proteomic Analyses-Recent Developments and Trends (2017–2021). *Micromachines* **2022**, *13*, 311. [CrossRef] [PubMed]
45. Schejbal, J.; Řemínek, R.; Zeman, L.; Mádr, A.; Glatz, Z. On-line coupling of immobilized cytochrome P450 microreactor and capillary electrophoresis: A promising tool for drug development. *J. Chromatogr. A* **2016**, *1437*, 234–240. [CrossRef] [PubMed]
46. Gkantzou, E.; Patila, M.; Stamatis, H. Magnetic Microreactors with Immobilized Enzymes—From Assemblage to Contemporary Applications. *Catalysts* **2018**, *8*, 282. [CrossRef]
47. Mandai, K.; Fukuda, T.; Miyazaki, Y.; Hashimoto, H.; Mandai, H.; Ema, T.; Takada, J.; Suga, S. Magnetic Attachment of Lipase Immobilized on Bacteriogenic Iron Oxide Inside a Microtube Reactor for the Kinetic Resolution of Secondary Alcohols. *Synlett* **2017**, *28*, 805–810. [CrossRef]
48. Sans, V. Emerging trends in flow chemistry enabled by 3D printing: Robust reactors, biocatalysis and electrochemistry. *Curr. Opin. Green Sustain. Chem.* **2020**, *25*, 100367. [CrossRef]
49. Shi, J.; Zhao, W.; Chen, Y.; Guo, L.; Yang, L. A replaceable dual-enzyme capillary microreactor using magnetic beads and its application for simultaneous detection of acetaldehyde and pyruvate. *Electrophoresis* **2012**, *33*, 2145–2151. [CrossRef]
50. Sheng, J.; Zhang, L.; Lei, J.; Ju, H. Fabrication of tunable microreactor with enzyme modified magnetic nanoparticles for microfluidic electrochemical detection of glucose. *Anal. Chim. Acta* **2012**, *709*, 41–46. [CrossRef]
51. Weiser, D.; Bencze, L.C.; Bánóczi, G.; Ender, F.; Kiss, R.; Kókai, E.; Szilágyi, A.; Vértessy, B.G.; Farkas, Ö.; Paizs, C.; et al. Phenylalanine Ammonia-Lyase-Catalyzed Deamination of an Acyclic Amino Acid: Enzyme Mechanistic Studies Aided by a Novel Microreactor Filled with Magnetic Nanoparticles. *ChemBioChem* **2015**, *16*, 2283–2288. [CrossRef]
52. Ender, F.; Weiser, D.; Nagy, B.; Bencze, C.L.; Paizs, C.; Pálovics, P.; Poppe, L. Microfluidic multiple cell chip reactor filled with enzyme-coated magnetic nanoparticles—An efficient and flexible novel tool for enzyme catalyzed biotransformations. *J. Flow Chem.* **2016**, *6*, 43–52. [CrossRef]
53. Hübner, J.; Brakowski, R.; Wohlgemuth, J.; Brenner-Weiß, G.; Franzreb, M. Compartmented microfluidic bioreactor system using magnetic enzyme immobilisates for fast small-scale biotransformation studies. *Eng. Life Sci.* **2015**, *15*, 721–726. [CrossRef]
54. Jussen, D.; Soltner, H.; Stute, B.; Wiechert, W.; von Lieres, E.; Pohl, M. µMORE: A microfluidic magnetic oscillation reactor for accelerated parameter optimization in biocatalysis. *J. Biotechnol.* **2016**, *231*, 174–182. [CrossRef] [PubMed]
55. Imarah, A.O.; Silva, F.M.W.G.; Tuba, L.; Malta-Lakó, Á.; Szemes, J.; Sánta-Bell, E.; Poppe, L. A Convenient U-Shape Microreactor for Continuous Flow Biocatalysis with Enzyme-Coated Magnetic Nanoparticles-Lipase-Catalyzed Enantiomer Selective Acylation of 4-(Morpholin-4-yl)butan-2-ol. *Catalysts* **2022**, *12*, 1065. [CrossRef]
56. Aldeghi, M.; Malhotra, S.; Selwood, D.L.; Chan, A.W.E. Two- and Three-dimensional Rings in Drugs. *Chem. Biol. Drug Des.* **2014**, *83*, 450–461. [CrossRef]
57. Lovering, F.; Bikker, J.; Humblet, C. Escape from Flatland: Increasing Saturation as an Approach to Improving Clinical Success. *J. Med. Chem.* **2009**, *52*, 6752–6756. [CrossRef]
58. Chen, C.S.; Fujimoto, Y.; Girdaukas, G.; Sih, C.J. Quantitative Analyses of Biochemical Kinetic Resolutions of Enantiomers. *J. Am. Chem. Soc.* **1982**, *104*, 7294–7299. [CrossRef]
59. Choi, J.H.; Choi, Y.K.; Kim, Y.H.; Park, E.S.; Kim, E.J.; Kim, M.-J.; Park, J. Aminocyclopentadienyl Ruthenium Complexes as Racemization Catalysts for Dynamic Kinetic Resolution of Secondary Alcohols at Ambient Temperature. *J. Org. Chem.* **2004**, *69*, 1972–1977. [CrossRef]
60. Toşa, M.; Pilbák, S.; Moldovan, P.; Paizs, C.; Szatzker, G.; Szakács, G.; Novák, L.; Irimie, F.-D.; Poppe, L. Lipase-catalyzed kinetic resolution of racemic 1-heteroarylethanols—Experimental and QM/MM study. *Tetrahedron Asymmetry* **2008**, *19*, 1844–1852. [CrossRef]
61. Hii, K.K.; Hellgardt, K. Catalysis in Flow: Why Leaching Matters. *Top. Organomet. Chem.* **2015**, *57*, 249–262. [CrossRef]

62. Csuka, P.; Molnár, Z.; Tóth, V.; Imarah, A.O.; Balogh-Weiser, D.; Vértessy, B.G.; Poppe, L. Immobilization of the Aspartate Ammonia-Lyase from *Pseudomonas fluorescens* R124 on Magnetic Nanoparticles: Characterization and Kinetics. *ChemBioChem* **2022**, *23*, e202100708. [CrossRef] [PubMed]
63. Rossi, D.; Pedrali, A.; Urbano, M.; Gaggeri, R.; Serra, M.; Fernandez, L.; Fernandez, M.; Caballero, J.; Ronsisvalle, S.; Prezzavento, O.; et al. Identification of a potent and selective σ1 receptor agonist potentiating NGF-induced neurite outgrowth in PC12 cells. *Bioorg. Med. Chem.* **2011**, *19*, 6210–6224. [CrossRef]
64. Kuriyama, M.; Nakashima, S.; Miyagi, T.; Sato, K.; Yamamoto, K.; Onomura, O. Palladium-catalyzed chemoselective anaerobic oxidation of *N*-heterocycle-containing alcohols. *Org. Chem. Front.* **2018**, *5*, 2364–2369. [CrossRef]
65. Ouyang, W.; Liu, B.; He, Y.; Wen, Y.; Gao, Y.; Huo, Y.; Chen, Q.; Li, X. Modular construction of functionalized anilines via switchable C-H and *N*-alkylations of traceless *N*-nitroso anilines with olefins. *Org. Chem. Front.* **2022**, *9*, 2746–2752. [CrossRef]
66. Deb, M.L.; Dey, S.S.; Bento, I.; Barros, M.T.; Maycock, C.D. Copper-catalyzed regioselective intramolecular oxidative α-functionalization of tertiary amines: An efficient synthesis of dihydro-1,3-oxazines. *Angew. Chem. Int. Ed.* **2013**, *52*, 9791–9795. [CrossRef] [PubMed]